Tensor-network simulations of bound states in perturbed quantum Ising chains

Part 1: Ground state properties

Frank Pollmann*, Markus Drescher, Shenghsuan Lin

December 17, 2020

Understanding the rich physics emerging in strongly interacting quantum matter requires the solution of challenging quantum many-body problems. Overcoming the exponential growth of complexity when simulating such quantum many-body systems is one of the most challenging goals in computational physics. For ground state properties of one-dimensional systems (1D) this challenge was answered by the introduction of matrix-product states (MPSs)—which provide a practically lossless compression of quantum states. Successively several MPS based algorithms have been introduced to efficiently simulate both ground states as well as dynamical properties. In this advanced practical training, you learn the basics of MPS based simulations and how to apply them to the quantum Ising chain. The goals of this lab course will be to (i) implement the time evolving block decimation (TEBD) algorithm to perform both real- and imaginary time evolution of the quantum Ising chain; (ii) obtain the phase diagram of the quantum Ising chain in a transverse field; (iii) calculate the dynamical spin structure factor in presence of both transverse and longitudinal fields. The dynamical spin structure factor is then compared to inelastic neutron scattering spectra of $CoNb_2O_6$.

*Department of Physics, Technical University of Munich, 85748 Garching, Germany, frank.pollmann@tum.de.

1 Introduction

The notion of quantum entanglement goes back to the early years of quantum mechanics and was subject of several papers by Schrödinger [1]. At the same time, Einstein, Podolski and Rosen discussed their famous "Gedankenexperiment" that attempted to show that quantum mechanical theory was incomplete [2]. Quantum entanglement is a physical phenomenon that occurs when particles interact in a way such that the quantum state of each particle cannot be described independently of the state of the others—including when the particles are separated by a large distance. For a long time, it was a topic discussed mostly in quantum optics and for systems with few degrees of freedom. In the last decades, however, it has seen a revival with input from very different areas, including the theory of black holes, quantum information and communication, the numerical investigation of quantum many-body systems, as well as the characterization of topological quantum states and quantum phase transitions. In this context, tensor-product state based methods have been shown to be a powerful tool to efficiently simulate quantum many-body systems if they are only slightly entangled. The most prominent algorithm in this context is the density matrix renormalization group (DMRG) method [3] which was originally conceived as an algorithm to study ground state properties of one-dimensional (1D) systems. A more recently introduced method that shares many similarities with DMRG is the time evolving block decimation (TEBD) method [4, 5, 6] that allows for an efficient time evolution of slightly entangled systems. In this practical training, we will use the TEBD method to investigate dynamical properties of a 1D quantum Ising chain that is relevant to describe inelastic Neuron scattering spectra of 1D materials such as $CoNb_2O_6$ [7].

2 Many-body entanglement

In the following, we introduce the concept of entanglement entropy and entanglement spectra in many-body systems. Let us consider the bipartition of the Hilbert space $\mathcal{H} = \mathcal{H}_A \otimes \mathcal{H}_B$ of an N-body quantum system as illustrated in Fig. 1(a), where $\mathcal{H}_A$ ($\mathcal{H}_B$) describes all the states defined in subsystem A and B, respectively.

We perform a so-called *Schmidt decomposition*, in which we decompose a (pure) state $|\Psi\rangle \in \mathcal{H}$ as

$$|\Psi\rangle = \sum_\alpha \Lambda_\alpha |\alpha\rangle_A \otimes |\alpha\rangle_B , \quad |\alpha\rangle_{A(B)} \in \mathcal{H}_{A(B)}, \tag{1}$$

where the states $\{|\alpha\rangle_{A(B)}\}$ form an orthonormal basis of (the relevant subspace of) $\mathcal{H}_A$ ($\mathcal{H}_B$) and $\Lambda_\alpha \geq 0$. The Schmidt decomposition is unique up to degeneracies and for a

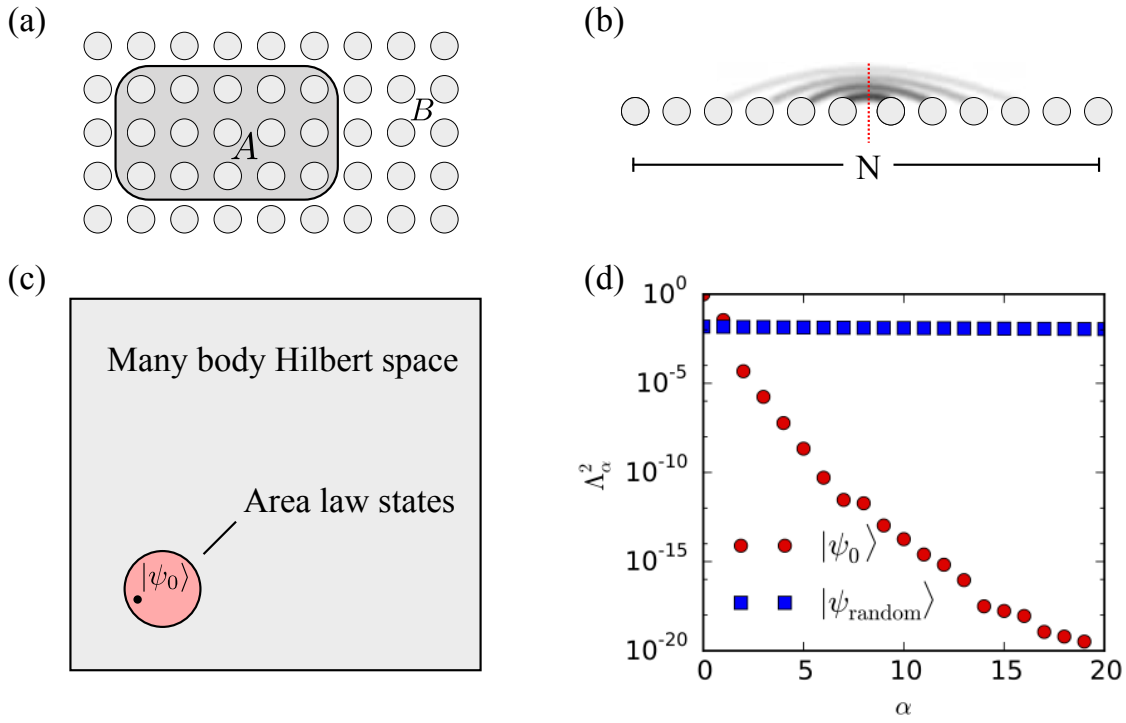

Figure 1: (a) Bipartition of a system into two parts A and B. The shaded area A has a boundary ∂A with surface area $|\partial A|$. (b) Significant quantum fluctuations in gapped ground states occur only on short length scales. (c) 1D area law states make up a very small fraction of the many-body Hilbert space but contain all gapped ground states. (d) Comparison of the largest Schmidt values of the ground state of the transverse field Ising model ($g = 1.5$) and a random state for a system consisting of $N = 16$ spins. The index α labels different Schmidt values.

normalized state $|\Psi\rangle$ we find that $\sum_\alpha \Lambda_\alpha^2 = 1$. Note that the Schmidt decomposition is equivalent to the singular-value decomposition of the coefficient matrix ψ_{ij} for chosen local bases $|i\rangle_A$ and $|i\rangle_B$, respectively. An important aspect of the Schmidt decomposition is that it gives direct insight into the *bipartite entanglement* (i.e., the quantum entanglement between degrees of freedom in $\mathcal{H}_A$ and $\mathcal{H}_B$) of a state: If no entanglement between the two subsystems is present, the state is a *product state* and the Schmidt decomposition has only one single non-zero Schmidt value ($\Lambda_1 = 1$ and $\Lambda_{\alpha>1} = 0$). If the degrees of freedom of the two subsystems are entangled, we necessarily have multiple non-zero Schmidt values in the decomposition.

A useful measure to quantify the amount of entanglement is the so-called *entanglement entropy*, which is defined as the von-Neumann entropy $S = -\mathrm{Tr}\left(\rho_A \log(\rho_A)\right)$ of the reduced density matrix ρ_A. The *reduced density matrix* of an entangled (pure) quantum state $|\psi\rangle$ is the density matrix of a mixed state defined on the subsystem,

$$\rho_A \equiv \mathrm{Tr}_B \left(|\psi\rangle \langle\psi|\right). \tag{2}$$

A simple calculation shows that it has the Schmidt states $|\alpha\rangle_A$ as eigenstates and the Schmidt coefficients are the square roots of the corresponding eigenvalues, i.e., $\rho_A = \sum_\alpha \Lambda_\alpha^2 |\alpha\rangle_A \langle\alpha|_A$ (equivalently for ρ_B). Hence, the entanglement entropy can be directly expressed in terms of the Schmidt values Λ_α,

$$S = -\mathrm{Tr}\left[\rho_A \log(\rho_A)\right] = -\sum_\alpha \Lambda_\alpha^2 \log \Lambda_\alpha^2. \tag{3}$$

Note that we would get the same entanglement entropy from the reduced density matrix ρ_B. If there is no entanglement between the two subsystems, we find $S = 0$ and $S > 0$ if there is any entanglement.

To demonstrate the concepts above, we consider a simple system consisting of two spin-1/2 with a bipartition in which the first spin is in subsystem A and the second in subsystem B.

The first example is a wave function

$$|\psi\rangle \;=\; \frac{1}{2}\left(|\uparrow\uparrow\rangle + |\uparrow\downarrow\rangle + |\downarrow\uparrow\rangle + |\downarrow\downarrow\rangle\right) \tag{4}$$

with Schmidt decomposition

$$|\psi\rangle \;=\; 1 \cdot [\frac{1}{\sqrt{2}}\left(|\uparrow\rangle + |\downarrow\rangle\right)] \otimes [\frac{1}{\sqrt{2}}\left(|\uparrow\rangle + |\downarrow\rangle\right)], \tag{5}$$

representing a product state with entanglement entropy $S = 0$. The second example is a wave function

$$|\psi\rangle \;=\; \frac{1}{\sqrt{2}}\left(|\uparrow\downarrow\rangle + |\downarrow\uparrow\rangle\right) \tag{6}$$

with Schmidt decomposition

$$|\psi\rangle \;=\; \frac{1}{\sqrt{2}} \cdot [|\uparrow\rangle \otimes |\downarrow\rangle] + \frac{1}{\sqrt{2}} \cdot [|\uparrow\rangle \otimes |\downarrow\rangle], \tag{7}$$

representing a maximally entangled state with entanglement entropy $S = \log 2$.

2.1 Area law

As we will discuss now, ground states of (gapped) local Hamiltonians are very special with respect to their entanglement properties—they fulfill an *area* law. It turns out that this allows on one hand for efficient numerical simulations and on the other hand provides the basis for the characterization of universal properties of quantum phases.

Let us first mention that a "typical" state in the Hilbert space has a *volume law*, i.e., the entanglement entropy grows proportionally with the volume of the partitions. In particular, it has been shown in Ref. [8] that in a system of N sites with on-site Hilbert space dimension d, a randomly drawn state $|\psi_{\text{random}}\rangle$ has an entanglement entropy of $S \approx N/2 \log d - 1/2$ for a bipartition into two parts of $N/2$ sites. Highly excited eigenstates of generic (ergodic) Hamiltonians typically show the same behavior.

In contrast, ground states $|\psi_0\rangle$ of gapped and local Hamiltonians follow an *area law*, i.e., the entanglement entropy grows proportionally to the area of the cut [15].[1]

$$S = \alpha |\partial A| + \ldots, \tag{8}$$

where α in the leading term is a non-universal coefficient and $|\partial A|$ denotes the surface area of the cut.

For the special case of a one dimensional chain of length N that is cut into two equal halves as shown in Fig. 1(b), this implies that $S(N)$ is constant for $N \gtrsim \xi$ (with ξ being the correlation length). This can be intuitively understood from the fact that a gapped ground state contains only fluctuations within the correlation length ξ and thus only degrees of freedom near the cut are entangled. A rigorous proof of the area law for 1D gapped and local Hamiltonians is given in Ref. [9]. Since typical states have a volume law, ground states are very special states and can be found within a very small corner of the Hilbert space, as illustrated in Fig. 1(c).

An important observation is that in slightly entangled states, only a relatively small number of Schmidt states contributes significantly to the weight of the state. This is demonstrated in Fig. 1(d) by comparing the largest 20 Schmidt values of an area law and a volume law state for a bipartition of an $N = 16$ chain into two half chains. As

[1] The condition of a gap can in certain cases be released but generically leads to sub-leading log corrections. In systems with a Fermi surface, the area law breaks down.

an example of an area law state, we considered here the ground state of the transverse field Ising model

$$H = -\sum_n \sigma_n^z \sigma_{n+1}^z + g\sigma_n^x, \tag{9}$$

with σ_n^x and σ_n^z being the Pauli operators and $g > 0$. This $\mathbb{Z}_2$ symmetric model has a quantum phase transition at $g_c = 1$. As shown in Fig. 1(d) for a representative example of $g = 1.5$, the entire weight of the ground state is essentially contained in a few Schmidt states. Generic states fulfilling the area law show a similar behavior and thus the above observation provides an extremely useful approach to compress quantum states by truncating the Schmidt decomposition. In particular, for all $\epsilon > 0$ we can truncate the Schmidt decomposition at some *finite* χ (independent of the system size) such that

$$\left\| |\psi\rangle - \underbrace{\sum_{\alpha=1}^{\chi} \Lambda_\alpha |\alpha\rangle_L \otimes |\alpha\rangle_R}_{|\psi^{\text{trunc}}\rangle} \right\| < \epsilon \tag{10}$$

This particular property of area law states is intimately related to the matrix-product state (MPS) representation of 1D quantum states, as we will discuss in the next chapter. The situation is very different for a highly entangled (volume law) random state: All the Schmidt values are roughly constant for all $2^{N/2}$ states and thus the 20 dominant states contain a vanishing weight (assuming an equal weight of configurations, we find $\Lambda_\alpha^2 \approx 1/2^{N/2}$ per Schmidt state).

3 Efficient representation and matrix-product states (MPSs)

We will now introduce MPSs [10, 11], which allow for an efficient representation of area law states in 1D. When working with MPSs, it is very helpful to use a diagrammatic tensor representation, which is illustrated in Fig. 2 (a) and (b). In this notation, a tensor with n indices is represented by a symbol with n legs.

We consider a chain with N sites and label the local basis on site n by $|j_n\rangle$ with $j_n = 1, \ldots, d$, e.g., for a spin-1/2 we have $d = 2$ local states $|\uparrow\rangle, |\downarrow\rangle$. Using the tensor product of local basis states, a generic (pure) quantum state can then be expanded as

$$|\psi\rangle = \sum_{j_1, j_2, \ldots j_N} \psi_{j_1 j_2 \cdots j_N} |j_1, j_2, \ldots, j_N\rangle . \tag{11}$$

Note that the order N tensor $\psi_{j_1,\ldots,j_n}$ has d^N complex entries which makes it prohibitively expensive to store or manipulate exactly even for moderate system sizes.

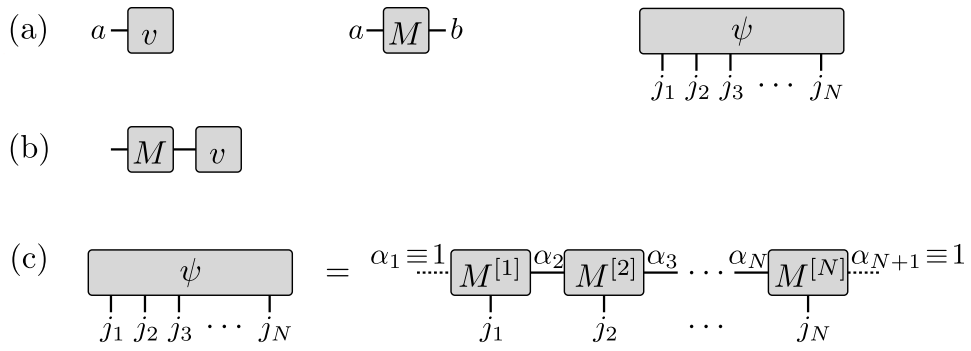

Figure 2: (a) Diagrammatic representations of a vector v, a matrix M, and the coefficients of a general many-body state $\psi_{j_1 j_2 \ldots j_n}$. (b) The connection of two legs symbolizes a tensor contraction, here $(Mv)_a = \sum_b M_{ab} v_b$, i.e., summing over the relevant indices. (c) The amplitude of the wave function is decomposed into a product of matrices $M^{[n]j_n}$. The indices α_1 and α_{N+1} are trivial, which we indicate by dashed lines.

For example, even on a large supercomputer, a simple $S = 1/2$ system with $d = 2$ can only be simulated exactly for up to $N \approx 40$ sites. Since numerical investigations of quantum-many body systems often require much larger systems, it is important to find ways to "compress" the quantum states to a manageable size—this is exactly what we will be able to do using MPS!

In an MPS, the coefficients $\psi_{j_1,\ldots,j_N}$ of a pure quantum state are decomposed into products of matrices of the form [10]:

$$|\psi\rangle = \sum_{j_1,\ldots,j_N} \sum_{\alpha_2,\ldots\alpha_N} M^{[1]j_1}_{\alpha_1\alpha_2} M^{[2]j_2}_{\alpha_2\alpha_3} \ldots M^{[N]j_N}_{\alpha_N\alpha_{N+1}} |j_1, j_2, \ldots, j_N\rangle \tag{12}$$

$$\equiv \sum_{j_1,\ldots,j_N} M^{[1]j_1} M^{[2]j_2} \ldots M^{[N]j_N} |j_1, j_2, \ldots, j_N\rangle \,. \tag{13}$$

Here, each $M^{[n]j_n}$ is a $\chi_n \times \chi_{n+1}$ dimensional matrix, i.e., we have a set of d matrices for each site, which we usually group into a tensor of order 3 as shown in Fig. 2(c). The superscript $[n]$ denotes the fact that for a generic state we have a different set of matrices on each site. The indices α_n of the matrices are called "bond", "virtual", or "auxiliary" indices, to distinguish them from the "physical" indices j_n. The matrices at the boundary are vectors, that is $\chi_1 = \chi_{N+1} = 1$, such that the matrix product in Eq. (13) produces a 1×1 matrix, i.e., a single number $\psi_{j_1,\ldots,j_N}$. It turns out that all area law states can be very well approximated by MPS with a finite bond dimension $\chi_{\max}$ [12, 13].

3.1 Simple examples of MPS

To become more familiar with the MPS notation, let us consider a few examples.

Product state: The state $|\psi\rangle = |\phi^{[1]}\rangle \otimes |\phi^{[2]}\rangle \otimes \cdots \otimes |\phi^{[n]}\rangle$ can easily be written in the form of Eq. (13); since it has no entanglement, the bond dimension is simply $\chi_n = 1$ on each bond and the 1×1 "matrices" are given by

$$M^{[n]j_n} = \left(\phi^{[n]}_{j_n}\right). \tag{14}$$

Concretely, the ground state of the transverse field Ising model given in Eq. (9) at infinite field $g \to \infty$ is a product state $|\leftarrow \cdots \leftarrow\rangle \equiv \left(\frac{1}{\sqrt{2}}|\uparrow\rangle - \frac{1}{\sqrt{2}}|\downarrow\rangle\right) \otimes \cdots \otimes \left(\frac{1}{\sqrt{2}}|\uparrow\rangle - \frac{1}{\sqrt{2}}|\downarrow\rangle\right)$, which we write as an MPS using the same set of matrices on each site n,

$$M^{[n]\uparrow} = \left(\tfrac{1}{\sqrt{2}}\right) \text{ and } \qquad M^{[n]\downarrow} = \left(\tfrac{-1}{\sqrt{2}}\right). \tag{15}$$

For the Neel state $|\uparrow\downarrow\uparrow\downarrow \ldots\rangle$, we need different sets of matrices on odd and even sites,

$$M^{[2n-1]\uparrow} = M^{[2n]\downarrow} = \big(1\big) \text{ and } \qquad M^{[2n-1]\downarrow} = M^{[2n]\uparrow} = \big(0\big) \tag{16}$$

for $n = 1, \ldots, N/2$.

Dimerized state: A product of singlets $\left(\frac{1}{\sqrt{2}}|\uparrow\downarrow\rangle - \frac{1}{\sqrt{2}}|\downarrow\uparrow\rangle\right) \otimes \cdots \otimes \left(\frac{1}{\sqrt{2}}|\uparrow\downarrow\rangle - \frac{1}{\sqrt{2}}|\downarrow\uparrow\rangle\right)$ on neighboring sites can be written with 1×2 matrices on odd sites and 2×1 matrices on even sites given by

$$M^{[2n-1]\uparrow} = \begin{pmatrix} \frac{1}{\sqrt{2}} & 0 \end{pmatrix}, \quad M^{[2n-1]\downarrow} = \begin{pmatrix} 0 & \frac{-1}{\sqrt{2}} \end{pmatrix}, \quad M^{[2n]\uparrow} = \begin{pmatrix} 0 \\ 1 \end{pmatrix}, \quad M^{[2n]\downarrow} = \begin{pmatrix} 1 \\ 0 \end{pmatrix}. \tag{17}$$

3.2 Canonical form

The MPS representation Eq. (13) is not unique. Consider the bond between sites n and $n+1$, which defines a bipartition into $L = \{1, \ldots, n\}$ and $R = \{n+1, \ldots, N\}$. Given an invertible $\chi_{n+1} \times \chi_{n+1}$ matrix X, we can replace

$$M^{[n]j_n} \to \tilde{M}^{[n]j_n} := M^{[n]j_n} X^{-1}, \qquad M^{[n+1]j_{n+1}} \to \tilde{M}^{[n+1]j_{n+1}} := X M^{[n+1]j_{n+1}} \tag{18}$$

and still represent the same state $|\psi\rangle$. This freedom can be used to define a convenient "canonical form" of the MPS, following Ref. [4, 6]. Without loss of generality, we can decompose the matrices $\tilde{M}^{[n]j_n} = \tilde{\Gamma}^{[n]j_n}\tilde{\Lambda}^{[n+1]}$, where $\tilde{\Lambda}^{[n+1]}$ is a square, diagonal

matrix with positive entries $\tilde{\Lambda}^{[n+1]}_{\alpha_{n+1}}$ on the diagonal. Performing partial contractions gives a representation looking very similar to the Schmidt decomposition (1):

$$\begin{aligned}|\psi\rangle &= \sum_{j_1,\dots,j_N} M^{[1]j_1}\dots M^{[n-1]j_{n-1}}\tilde{\Gamma}^{[n]j_n}\tilde{\Lambda}^{[n+1]}\tilde{M}^{[n+1]j_{n+1}}M^{[n+2]j_{n+2}}\dots M^{[N]j_N}\,|j_1,\dots,j_N\rangle \\ &= \sum_{\tilde{\alpha}_{n+1}} \tilde{\Lambda}^{[n+1]}_{\tilde{\alpha}_{n+1}}\,|\tilde{\alpha}_{n+1}\rangle_L \otimes |\tilde{\alpha}_{n+1}\rangle_R\,, \text{ where} \qquad (19)\end{aligned}$$

$$|\tilde{\alpha}_{n+1}\rangle_L = \sum_{j_1,\dots,j_n} \left(M^{[1]j_1}\dots M^{[n-1]j_{n-1}}\tilde{\Gamma}^{[n]j_n}\right)_{1,\tilde{\alpha}_{n+1}} |j_1,\dots,j_n\rangle\,, \qquad (20)$$

$$|\tilde{\alpha}_{n+1}\rangle_R = \sum_{j_{n+1},\dots,j_N} \left(\tilde{M}^{[n+1]j_{n+1}}M^{[n+2]j_{n+2}}\dots M^{[N]j_N}\right)_{\tilde{\alpha}_{n+1},1} |j_{n+1},\dots,j_N\rangle\,. \qquad (21)$$

However, for general M and $\tilde{\Gamma}^{[n]}$, the states $|\tilde{\alpha}_{n+1}\rangle_{L/R}$ will not be orthonormal. Note that we can interpret the X in Eq. (18) as a basis transformation of the states $|\tilde{\alpha}_{n+1}\rangle_R$ in Eq. (21). The idea of the canonical form is to choose the X in Eq. (18) such that it maps $|\tilde{\alpha}_{n+1}\rangle_R$ to the Schmidt states $|\alpha_{n+1}\rangle_R$. Using the Schmidt values $\Lambda^{[n+1]}_{\alpha_{n+1}}$ on the diagonal of $\tilde{\Lambda}^{[n+1]} \to \Lambda^{[n+1]}$, we find that Eq. (19) indeed gives the Schmidt decomposition. Repeating this on each bond yields the canonical form

$$|\Psi\rangle = \sum_{j_1,\dots,j_N} \Lambda^{[1]}\Gamma^{[1]j_1}\Lambda^{[2]}\Gamma^{[2]j_2}\Lambda^{[3]}\dots\Lambda^{[N]}\Gamma^{[N]j_N}\Lambda^{[N+1]}\,|j_1,\dots,j_N\rangle\,. \qquad (22)$$

Here, we have introduced trivial 1×1 matrices $\Lambda^{[1]} \equiv \Lambda^{[N+1]} \equiv \big(1\big)$ multiplied to the trivial legs of the first and last tensor, again with the goal to achieve a uniform bulk. While the canonical form is useful as it allows to quickly read off the Schmidt decomposition on any bond, in practice we usually group each Γ with one of the Λ matrices and define

$$A^{[n]j_n} \equiv \Lambda^{[n]}\Gamma^{[n]j_n}, \qquad\qquad B^{[n]j_n} \equiv \Gamma^{[n]j_n}\Lambda^{[n+1]}. \qquad (23)$$

If we write an MPS entirely with A tensors (B tensors), it is said to be in left (right) canonical form. If we consider the bond between sites n and $n+1$, we can write the MPS in a "mixed" canonical form with A tensors up to site n and B tensors starting from site $n+1$. The A and B tensors transform the Schmidt basis from one bond to the next:

$$|\alpha_{n+1}\rangle_L = \sum_{\alpha_n,j_n} A^{[n]j_n}_{\alpha_n\alpha_{n+1}}\,|\alpha_n\rangle_L \otimes |j_n\rangle\,, \quad |\alpha_n\rangle_R = \sum_{j_n,\alpha_{n+1}} B^{[n]j_n}_{\alpha_n\alpha_{n+1}}\,|j_n\rangle \otimes |\alpha_{n+1}\rangle_R\,, \quad (24)$$

with orthonormality conditions $\langle\alpha_n|_L\,|\bar{\alpha}_n\rangle_L = \delta_{\alpha_n\bar{\alpha}_n} = \langle\alpha_n|_R\,|\bar{\alpha}_n\rangle_R$.

One great advantage of the canonical form is that these relations allow to evaluate expectation values of local operators very easily. If needed, we can easily convert the left and right canonical forms into each other, e.g., $A^{[n]} = \Lambda^{[n]} B^{[n]} \left(\Lambda^{[n+1]}\right)^{-1}$; since the $\Lambda^{[n]}$ are diagonal matrices, their inverses are simply given by diagonal matrices with the inverse Schmidt values[2].

3.3 Time Evolving Block Decimation (TEBD)

Now that we know how to represent quantum states as MPS, we would like to manipulate them and use them for studying microscopic models. A very useful algorithm is the Time Evolving Block Decimation (TEBD) algorithm [5], which allows evaluating the time evolution of an MPS:

$$|\psi(t)\rangle = U(t)\,|\psi(0)\rangle\,. \tag{25}$$

The time evolution operator U can either be $U(t) = \exp(-itH)$ yielding a real time evolution, or an imaginary time evolution $U(\tau) = \exp(-\tau H)$. The latter can be used to evaluate (finite temperature) Green's functions or as a first, conceptually simple way to find the ground state of the Hamiltonian H through the relation

$$|\psi_{\mathrm{GS}}\rangle = \lim_{\tau\to\infty} \frac{e^{-\tau H}\,|\psi_0\rangle}{\|e^{-\tau H}\,|\psi_0\rangle\|}. \tag{26}$$

The TEBD algorithm makes use of the Suzuki-Trotter decomposition [14], which approximates the exponent of a sum of operators with a product of exponents of the same operators. For example, the first and second order expansions read

$$e^{(X+Y)\delta} = e^{X\delta}e^{Y\delta} + \mathcal{O}(\delta^2), \tag{27}$$

$$e^{(X+Y)\delta} = e^{X\delta/2}e^{Y\delta}e^{X\delta/2} + \mathcal{O}(\delta^3). \tag{28}$$

Here X and Y are operators, and δ is a small parameter. To make use of these expressions, we assume that the Hamiltonian is a sum of two-site operators of the form $H = \sum_n h^{[n,n+1]}$, where $h^{[n,n+1]}$ acts only on sites n and $n+1$, and decompose it as a sum

$$H = \underbrace{\sum_{n \text{ odd}} h^{[n,n+1]}}_{H_{\mathrm{odd}}} + \underbrace{\sum_{n \text{ even}} h^{[n,n+1]}}_{H_{\mathrm{even}}}. \tag{29}$$

[2] If $\Lambda^{[n+1]}_{\alpha_{n+1}\alpha_{n+1}} = 0$ for some α_{n+1}, we can remove the corresponding columns of $B^{[n]}$ and rows of $B^{[n+1]}$ before taking the inverse, as they do not contribute to the wave function.

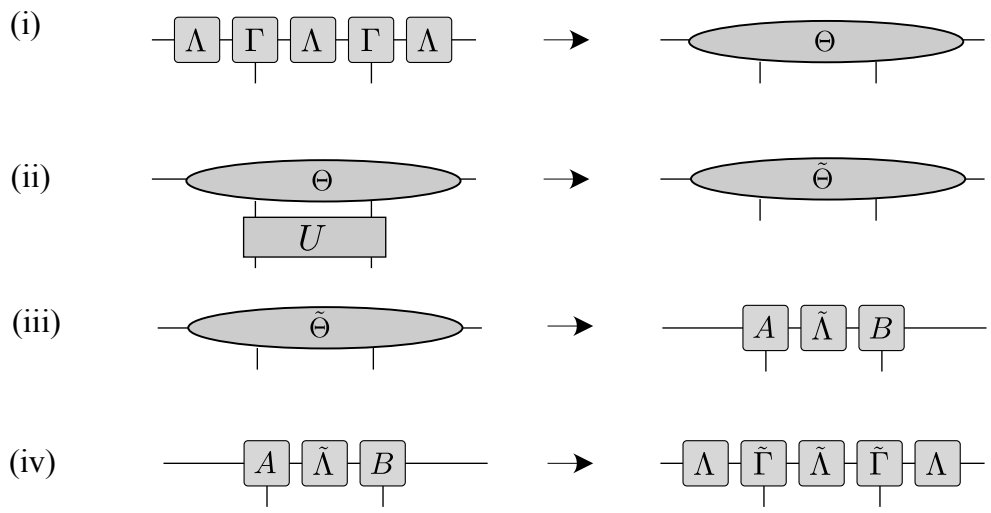

Figure 3: Update to apply a two-site unitary U and recover the canonical MPS form (see text for details). Note that we do not explicitly label the positions of the individual tensors in favor for a less cluttered presentation.

Each term H_{odd} and H_{even} consists of a sum of commuting operators, therefore $e^{H_{\text{odd}}\delta} = \prod_{n \text{ odd}} e^{h^{[n,n+1]}\delta}$ and similar for H_{even}. We now divide the time into small time slices $\delta t \ll 1$ (the relevant time scale is in fact the inverse gap) and consider a time evolution operator $U(\delta t)$. Using, as an example, the first order decomposition (27), the operator $U(\delta t)$ can be expanded into products of two-site unitary operators

$$U(\delta t) \approx \left[\prod_{n \text{ odd}} U^{[n,n+1]}(\delta t)\right]\left[\prod_{n \text{ even}} U^{[n,n+1]}(\delta t)\right], \tag{30}$$

where $U^{[n,n+1]}(\delta t) = e^{-\mathrm{i}\,\delta t\, h^{[n,n+1]}}$. The successive application of these two-site unitary operators to an MPS is the main part of the algorithm and explained in the following.

Local unitary updates of an MPS. One of the advantages of the MPS representation is that local transformations can be performed efficiently. Moreover, the canonical form discussed above is preserved if the transformations are unitary [4].

A one-site unitary U simply transforms the tensors Γ of the MPS

$$\tilde{\Gamma}^{[n]j_n}_{\alpha_n\alpha_{n+1}} = \sum_{j'_n} U^{j_n}_{j'_n} \Gamma^{[n]j'_n}_{\alpha_n\alpha_{n+1}}. \tag{31}$$

In such a case the entanglement of the wave-function is not affected and thus the values of Λ do not change. The update procedure for a two-site unitary transformation acting on two neighboring sites n and $n+1$ is shown in Fig. 3. We first find the wave function in the basis spanned by the left Schmidt states $|\alpha_n\rangle_L$, the local basis $|j_n\rangle$ and $|j_{n+1}\rangle$ on sites n and $n+1$, and the right Schmidt states $|\alpha_{n+2}\rangle_R$, which together form an orthonormal basis $\{\ |\alpha_n\rangle_L \otimes\ |j_n\rangle \otimes\ |j_{n+1}\rangle \otimes\ |\alpha_{n+2}\rangle_R\}$. Calling the wave function coefficients Θ, the state is expressed in a mixed bases as

$$|\psi\rangle = \sum_{\alpha_n, j_n, j_{n+1}, \alpha_{n+2}} \Theta^{j_n j_{n+1}}_{\alpha_n \alpha_{n+2}} |\alpha_n\rangle_L |j_n\rangle |j_{n+1}\rangle |\alpha_{n+2}\rangle_R . \tag{32}$$

Using the definitions of the canonical form, Θ is given by

$$\Theta^{j_n j_{n+1}}_{\alpha_n \alpha_{n+2}} = \sum_{\alpha_{n+1}} \Lambda^{[n]}_{\alpha_n} \Gamma^{[n], j_n}_{\alpha_n \alpha_{n+1}} \Lambda^{[n+1]}_{\alpha_{n+1}} \Gamma^{[n+1], j_{n+1}}_{\alpha_{n+1} \alpha_{n+2}} \Lambda^{[n+2]}_{\alpha_{n+2}}. \tag{33}$$

Writing the wave function in this basis is useful because it is easy to apply the two-site unitary in step (ii) of the algorithm:

$$\tilde{\Theta}^{j_n j_{n+1}}_{\alpha_n \alpha_{n+2}} = \sum_{j'_n j'_{n+1}} U^{j_n j_{n+1}}_{j'_n j'_{n+1}} \Theta^{j'_n j'_{n+1}}_{\alpha_n \alpha_{n+2}}. \tag{34}$$

Next we have to extract the new tensors $\tilde{B}^{[n]}, \tilde{B}^{[n+1]}$ and $\tilde{\Lambda}^{[n+1]}$ from the transformed tensor $\tilde{\Theta}$ in a manner that preserves the canonical form. We first "reshape" the tensor $\tilde{\Theta}$ by combining indices to obtain a $d\chi_n \times d\chi_{n+2}$ dimensional matrix $\tilde{\Theta}_{j_n \alpha_n ; j_{n+1} \alpha_{n+2}}$. Because the basis $\{\ |\alpha_n\rangle_L \otimes\ |j_n\rangle\ \}$ is orthonormal, as for the right, it is natural to decompose the matrix using the singular value decomposition (SVD) in step (iii) into

$$\tilde{\Theta}_{j_n \alpha_n ; j_{n+1} \alpha_{n+2}} = \sum_{\alpha_{n+1}} \tilde{A}^{[n]}_{j_n \alpha_n ; \alpha_{n+1}} \tilde{\Lambda}^{[n+1]}_{\alpha_{n+1} \alpha_{n+1}} \tilde{B}^{[n+1]}_{\alpha_{n+1} ; j_{n+1} \alpha_{n+2}}, \tag{35}$$

where $\tilde{A}^{[n]}, \tilde{B}^{[n+1]}$ are isometries and $\tilde{\Lambda}^{[n+1]}$ is a diagonal matrix. Indeed, the suggestive notation that the new tensors are in mixed canonical form is justified, since the SVD yields a Schmidt decomposition of the wave function for a bipartition at the bond between sites n and $n+1$. The isometry $\tilde{A}^{[n]}$ relates the new Schmidt states $|\alpha_{n+1}\rangle_L$ to the combined bases $|\alpha_n\rangle_L \otimes |j_n\rangle$. Analogously, the Schmidt states for the right site are obtained from the matrix $B^{[n+1]}$. Thus the diagonal matrix $\tilde{\Lambda}^{[n+1]}$ contains precisely the Schmidt values of the transformed state. In a last step (iv), we reshape the obtained matrices $\tilde{A}^{[n]}, \tilde{B}^{[n+1]}$ back to tensors with 3 indices and recover the right canonical form by

$$\tilde{\Gamma}^{[n] j_n}_{\alpha_n \alpha_{n+1}} = (\Lambda^{[n]})^{-1}_{\alpha_n} \tilde{A}^{[n]}_{j_n \alpha_n ; \alpha_{n+1}} \qquad \text{and} \qquad \tilde{\Gamma}^{[n+1] j_{n+1}}_{\alpha_{n+1} \alpha_{n+2}} = \tilde{B}^{[n+1]}_{\alpha_{n+1} ; j_{n+1} \alpha_{n+2}} (\Lambda^{[n+2]})^{-1}_{\alpha_{n+2}}. \tag{36}$$

After the update, the new MPS is still in the canonical form. The entanglement at the bond $n, n+1$ has changed and the bond dimension increased to $d\chi$. Thus the amount of information in the wave function grows exponentially if we successively apply unitaries to the state. To overcome this problem, we perform an approximation by fixing the maximal number of Schmidt terms to $\chi_{\max}$. In each update, only the $\chi_{\max}$ most important states are kept in step (iii), i.e., if we order the Schmidt states according to their size we simply truncate the range of the index α_{n+1} in Eq. (35) to be $1 \dots \chi_{\max}$. This approximation limits the dimension of the MPS and the tensors B have at most a dimension of $\chi_{\max} \times d \times \chi_{\max}$. Given that the truncated weight is small, the normalization conditions for the canonical form will be fulfilled to a good approximation. In order to keep the wave function normalized, one should divide by the norm after the truncation, i.e., divide by $\mathcal{N} = \sqrt{\sum_{j_n, j_{n+1}, \alpha_n, \alpha_{n+2}} \left|\Theta^{j_n j_{n+1}}_{\alpha_n \alpha_{n+2}}\right|^2}$.

Using the TEBD algorithm, we can now perform real and imaginary time evolution of MPS. While the imaginary time evolution provides a tool to find ground states, it turns out that a variational optimization is often more efficient. This is done using the density-matrix renormalization group (DMRG) method [3]. The DMRG replaces step (ii) in the TEBD algorithm, in which the two site gate is applied, with a variational optimization of the local tensors. This can be done using for example the Lanczos algorithm.

4 Numerical Procedure

We investigate the phase diagram and dynamical properties of the quantum Ising model in a transverse and longitudinal field,

$$H = -J \sum_n \sigma^x_n \sigma^x_{n+1} - g \sum_n \sigma^z_n - h \sum_n \sigma^x_n. \tag{37}$$

4.1 Implementation of the TEBD algorithm

This exercise uses the provided files `a_mps.py, b_model.py, c_tebd.py`.

a) Read the code in the file `a_mps.py`. This file defines the class `MPS` in an object-oriented approach. In short, defining the class is defining a "type" which collects data in attributes (e.g. `MPS.Bs, MPS.L`) and has methods (e.g. `MPS.site_expectation_value`) which can use the attributes (referenced with the special first argument `self`) for calculations. Generate an *instance* of the MPS class representing the state $|\uparrow\uparrow \dots \uparrow\rangle$ with the function `init_spinup_MPS`, for the start with $L = 14$ sites.

Check that the (site) expectation values of the operators $\sigma^z = \begin{pmatrix} 1 & 0 \\ 0 & -1 \end{pmatrix}$ and $\sigma^x = \begin{pmatrix} 0 & 1 \\ 1 & 0 \end{pmatrix}$ give the expected values.

b) Write a function similar to `init_spinup_MPS`, but initialize an MPS for the state $|{\rightarrow}{\rightarrow}\cdots{\rightarrow}\rangle$. Check the expectation values again.

Hint: This state is also a product state of $|{\rightarrow}\rangle = \frac{1}{\sqrt{2}}(|{\uparrow}\rangle + |{\downarrow}\rangle)$, so the singular values remain the same and the shape of each `B` is still (1,2,1). You should expect rounding errors of the order of machine precision $\approx 10^{-15}$.

c) Read the file `b_model.py`. It defines a class representing the transverse field ising model for a given choice of coupling parameters. Calculate the energy for $L = 14, J = 1$ and $g \in \{\, 0.5, 1, 1.5 \,\}$ for each of the above defined two product states. For later usage, extend the model or write a new model class which also includes the longitudinal field h.

d) Read the file `c_tebd.py`, which implements the time evolving block decimation. Call the function `example_TEBD_gs_finite`, which performs an imaginary time evolution to project onto the ground state.

4.2 Ground state Phase diagram

Obtain the phase diagram of the quantum Ising model as function of g at $h = 0$ using the TEBD algorithm in imaginary time.

a) Write a function to (efficiently) calculate (equal-time) correlation functions like $\langle\psi| X_i Y_j |\psi\rangle$ for some single-site operators X, Y, which are applied on sites i and j, respectively. The functions should take $|\psi\rangle, X, Y$ and i as an input and calculate the correlations $\langle\psi| X_i Y_j |\psi\rangle$ for all $j \geq i$.

Hint: Distinguish the cases $i = j$ and $i < j$. Assume that $|\psi\rangle$ is given in right canonical B form (since our DMRG implementation returns it as such). Use the orthonormality conditions of the canonical form on sites k for $k < i$ (left canonical form) and $k > j$ to simplify the expression of the correlation function to the following network (for $i < j$):

$\langle\psi| X_i Y_j |\psi\rangle =$ 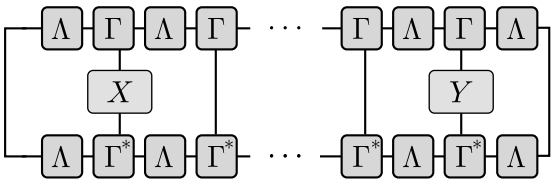

(38)

To keep track of the indices which you need to contract with `np.tensordot`, it can help to draw diagrams and label the legs. It is possible to write the function with a computational cost of $\mathcal{O}((L-i)^1)$, i.e., a single for loop of j.

b) Run TEBD in imaginary time for some values of g and $L = 30$ (e.g. $g = 0.3, 0.5, 0.8, 0.9, 1., 1.1, 1.2, 1.5$). Calculate and plot the correlations $\langle \sigma^x_{L/4} \sigma^x_j \rangle$. Does it agree with your expectations? How do the correlations decay at $g = 1$ and $g > 1$?

c) Plot the phase transition in the order parameter m (magnetization) by using the relation

$$\langle \sigma^x_i \sigma^x_j \rangle \to m^2 \text{ for } |i-j| \to \infty \,, \tag{39}$$

meaning that the correlations approach a constant value of the magnetization squared for large distances. Make sure to exclude boundary effects.

d) (optional) Plot the connected correlations $C(j) = \langle \sigma^x_{L/4} \sigma^x_j \rangle - \langle \sigma^x_{L/4} \rangle \langle \sigma^x_j \rangle$ versus $j - L/4$ on a logarithmic y-scale. For $g > 1$, extract the correlation length ξ by a fit $C(j) \propto \exp(-\frac{|j-L/4|}{\xi})$.

Hint: Again, you can use `np.polyfit` if you fit $\log(C(j))$ vs. $|j - L/4|$.

References

[1] E. Schrödinger, Proceedings of the Cambridge Philosophical Society **31**, 555 (1935)

[2] A. Einstein, B. Podolsky, and N. Rosen, Phys. Rev. **47**, 777 (1935)

[3] S. R. White, Phys. Rev. Lett. **69**, 2863 (1992)

[4] G. Vidal, J. I. Latorre, E. Rico, and A. Kitaev, Phys. Rev. Lett. **90**, 227902 (2003)

[5] G. Vidal, Phys. Rev. Lett. **93**, 040502 (2004)

[6] G. Vidal, Phys. Rev. Lett. **98**, 070201 (2007)

[7] R. Coldea, D. A. Tennant, E. M. Wheeler, E. Wawrzynska, D. Prabhakaran, M. Telling, K. Habicht, P. Smeibidl, and K. Kiefer, Science **327**, 177 (2010)

[8] D. N. Page, Phys. Rev. Lett. **71**, 1291 (1993)

[9] M. B. Hastings, J. Stat. Mech. Theory Exp. **2007**, P08024 (2007)

[10] M. Fannes, B. Nachtergaele, and R. F. Werner, Commun. Math. Phys. **144**, 443 (1992)

[11] U. Schollwöck, Ann. Phys. (N. Y). **326**, 96 (2011)

[12] D. Gottesman and M. B. Hastings, New J. Phys. **12**, 025002 (2010)

[13] N. Schuch, M. M. Wolf, F. Verstraete, and J. I. Cirac, Phys. Rev. Lett. **100**, 030504 (2008)

[14] M. Suzuki, J. Math. Phys. **32**, 400 (1991)

[15] J. Eisert, M. Cramer, and M. B. Plenio, Rev. Mod. Phys. **82**, 277 (2010)

[16] B. M. McCoy and T. T. Wu, Phys. Rev. D **18**, 1259 (1978)

Tensor-network simulations of bound states in perturbed quantum Ising chains

Part 2: Dynamic spin structure factor

Frank Pollmann*, Markus Drescher, Shenghsuan Lin

December 17, 2020

1 Dynamic spin structure factors

1.1 Introduction

The quantities we are interested in are the dynamic (spin) structure factors (DSF) also referred to as the spectral functions. In this note, we give the definition, the interpretation and how to compute such quantities in practice. A general introduction with reference to experiments and some numerical scheme can be found here.

The dynamic structure factor is of special importance for several reasons. It gives us direct insight into the spectrum of the Hamiltonian and the physical properties of the quasi-particles. Basically speaking, the dynamic structure factor provides information about the excitations of the system. If the system considered is in the ground state, the dynamic structure factor then tells you about the excitations above the ground state.

The dynamic structure factor can be measured by inelastic neutron scattering in experiment and can be computed using various methods in theory. As a result, it is a quantity of interest from both theoretical and experimental perspective.

*Department of Physics, Technical University of Munich, 85748 Garching, Germany, frank.pollmann@tum.de.

1.2 The dynamic structure factor

Physical systems usually are translationally invariant. As a result, we could define the Fourier transform of an operator as,

$$\hat{O}^{\alpha}_{\mathbf{k}} = \frac{1}{\sqrt{N}} \sum_{\mathbf{r}} e^{-i\mathbf{k}\cdot\mathbf{r}} \hat{O}^{\alpha}_{\mathbf{r}} \qquad \hat{O}^{\alpha}_{\mathbf{r}} = \frac{1}{\sqrt{N}} \sum_{\mathbf{k}} e^{i\mathbf{k}\cdot\mathbf{r}} \hat{O}^{\alpha}_{\mathbf{k}}\,, \tag{1}$$

where the sum over $\mathbf{r}$ is running over all lattice sites and the sum over $\mathbf{k}$ is running over all k-points, which depend on the underlying lattice structure.

Definition The dynamic spin structure factor is defined in momentum and frequency space as follows:

$$\begin{aligned} S^{\alpha\beta}(\mathbf{k},\omega) &= \frac{1}{2\pi} \int_{-\infty}^{\infty} e^{i\omega t} \left\langle (\hat{O}^{\alpha}_{-\mathbf{k}})^{\dagger}(t) \hat{O}^{\beta}_{-\mathbf{k}}(0) \right\rangle dt & (2)\\ &= \frac{1}{2\pi N} \sum_{\mathbf{r},\mathbf{r}'} e^{-i\mathbf{k}\cdot(\mathbf{r}-\mathbf{r}')} \int_{-\infty}^{\infty} e^{i\omega t} \left\langle \hat{O}^{\alpha\dagger}_{\mathbf{r}}(t) \hat{O}^{\beta}_{\mathbf{r}'}(0) \right\rangle dt & (3)\\ &= \frac{1}{2\pi} \sum_{\mathbf{R}} e^{-i\mathbf{k}\cdot\mathbf{R}} \int_{-\infty}^{\infty} e^{i\omega t} \left\langle \hat{O}^{\alpha\dagger}_{\mathbf{R}}(t) \hat{O}^{\beta}_{\mathbf{0}}(0) \right\rangle dt & (4) \end{aligned}$$

It is obtained from the double Fourier transformation of the real-time correlation function $\langle \hat{O}^{\alpha\dagger}_{\mathbf{R}}(t) \hat{O}^{\beta}_{\mathbf{0}}(0) \rangle$ in both space and time. From the definition, it follows that $S^{\alpha\beta}(\mathbf{k},\omega) = (S^{\beta\alpha}(\mathbf{k},\omega))^*$. The quantity we are mainly interested in is $S^{\alpha\alpha}(\mathbf{k},\omega)$, which is hence *real*.

Lehmann representation In fact, $S^{\alpha\alpha}(\mathbf{k},\omega)$ would not only be *real* but also *positive*. The reason why it is positive can be understood from the so-called *Lehmann representation* or the spectral form,

$$\boxed{S^{\alpha\alpha}(\mathbf{k},\omega) = \sum_{n} \delta(\omega - (\omega_n - \omega_0)) |\langle n|\hat{O}^{\alpha}_{-\mathbf{k}}|0\rangle|^2} \tag{5}$$

This nice form can be obtained as follows,

$$\begin{aligned}
S^{\alpha\alpha}(\mathbf{k},\omega) &= \frac{1}{2\pi}\int_{-\infty}^{\infty} e^{i\omega t}\Big\langle \mathcal{U}^\dagger(t)(\hat{O}^\alpha_{-\mathbf{k}})^\dagger \mathcal{U}(t)\hat{O}^\alpha_{-\mathbf{k}}(0)\Big\rangle dt \\
&= \frac{1}{2\pi}\int_{-\infty}^{\infty} e^{i(\omega+\omega_0)t}\Big\langle (\hat{O}^\alpha_{-\mathbf{k}})^\dagger \mathcal{U}(t)\Big(\sum_n |n\rangle\langle n|\Big)\hat{O}^\alpha_{-\mathbf{k}}(0)\Big\rangle dt \\
&= \sum_n \frac{1}{2\pi}\int_{-\infty}^{\infty} e^{i(\omega-(\omega_n-\omega_0))t}\langle 0|\,(\hat{O}^\alpha_{-\mathbf{k}})^\dagger\,|n\rangle\langle n|\,\hat{O}^\alpha_{-\mathbf{k}}\,|0\rangle\, dt \\
&= \sum_n \delta(\omega-(\omega_n-\omega_0))|\langle n|\hat{O}^\alpha_{-\mathbf{k}}|0\rangle|^2
\end{aligned}$$

In the second equality, we insert a resolution of identity $\mathbb{1} = \sum_n |n\rangle\langle n|$, where n runs over all energy eigenstates.

The Lehmann representation of the dynamic structure factor tells us that if $S^{\alpha\alpha}(\mathbf{k},\omega) \neq 0$, then there exists an energy eigenstate with energe ω and the eigenstate has non-zero overlap with $\hat{O}^\alpha_{-\mathbf{k}}$ acting on the ground state.

1.3 Numerical Methods

In practice, to compute $S^{\alpha\alpha}$ numerically, we have to adjust the formula a bit more.

1. (Exact) We rewrite the integral so the limit runs from 0 to ∞.
2. (Approximation) Discretize the time steps
3. (Tricks) Gaussian windowing

Rewrite Integral In practice, when doing the calculation, we don't want to evolve the states to (minus) infinity. In fact, we can rewrite the expression *exactly* and get rid of one side of the limit. This makes it easier to work with. The expression is given as,

$$\boxed{S^{\alpha\alpha}(\mathbf{k},\omega) = \frac{1}{2\pi}\sum_{\mathbf{R}} e^{-i\mathbf{k}\cdot\mathbf{R}}\int_0^\infty 2\mathrm{Re}\left[e^{i\omega t}\langle \hat{O}^{\alpha\dagger}_{\mathbf{R}}(t)\hat{O}^\alpha_{\mathbf{0}}(0)\rangle\right] dt} \tag{6}$$

See the derivation below.

$$\begin{aligned}
\int_{-\infty}^{\infty} dt e^{i\omega t}\langle \hat{O}^{\alpha\dagger}_{\mathbf{R}}(t)\hat{O}^\alpha_{\mathbf{0}}(0)\rangle &= \int_0^\infty dt e^{i\omega t}\langle \hat{O}^{\alpha\dagger}_{\mathbf{R}}(t)\hat{O}^\alpha_{\mathbf{0}}(0)\rangle + \int_{-\infty}^0 dt e^{i\omega t}\langle \hat{O}^{\alpha\dagger}_{\mathbf{R}}(t)\hat{O}^\alpha_{\mathbf{0}}(0)\rangle \\
&= \int_0^\infty dt e^{i\omega t}\langle \hat{O}^{\alpha\dagger}_{\mathbf{R}}(t)\hat{O}^\alpha_{\mathbf{0}}(0)\rangle + \int_0^\infty dt e^{-i\omega t}\langle \hat{O}^{\alpha\dagger}_{\mathbf{R}}(-t)\hat{O}^\alpha_{\mathbf{0}}(0)\rangle \\
&= \int_0^\infty dt\left[e^{i\omega t}\langle \hat{O}^{\alpha\dagger}_{\mathbf{R}}(t)\hat{O}^\alpha_{\mathbf{0}}(0)\rangle + \Big(e^{i\omega t}\langle \hat{O}^{\alpha\dagger}_{\mathbf{0}}(t)\hat{O}^\alpha_{\mathbf{R}}(0)\rangle\Big)^*\right]
\end{aligned}$$

where for the second equality we use, $\int_a^b f(t)dt = \int_{-b}^{-a} f(-t)dt$. The third equality follows from the following properties,

$$\begin{aligned} Tr[\rho\hat{O}^{\alpha\dagger}(-t)\hat{O}^{\alpha}(0)] &= Tr[\rho\mathcal{U}\hat{O}^{\alpha\dagger}(0)\mathcal{U}^{\dagger}\hat{O}^{\alpha}(0)] \\ &= Tr[\rho\hat{O}^{\alpha\dagger}(0)\mathcal{U}^{\dagger}\hat{O}^{\alpha}(0)\mathcal{U}] \\ &= Tr[\rho\hat{O}^{\alpha\dagger}(0)\hat{O}^{\alpha}(t)]\,, \end{aligned}$$

where $\rho = |\psi_0\rangle\langle\psi_0|$ is the density matrix of the eigenstate so that $\rho\mathcal{U} = \mathcal{U}\rho$.

By evoking the translation invariance of the system, we have shifted the correlation from between $\mathbf{0}$ and $\mathbf{R}$ to between $-\mathbf{R}$ and $\mathbf{0}$. Since the sum over $\mathbf{R}$ runs over all possible positions, we can rearrange the sum and arrive at the final formula.

$$\begin{aligned} S^{\alpha\alpha}(\mathbf{k},\omega) &= \frac{1}{2\pi}\sum_{\mathbf{R}} e^{-i\mathbf{k}\cdot\mathbf{R}} \int_0^{\infty} \left[e^{i\omega t}\langle\hat{O}^{\alpha\dagger}_{\mathbf{R}}(t)\hat{O}^{\alpha}_{\mathbf{0}}(0)\rangle + \left(e^{i\omega t}\langle\hat{O}^{\alpha\dagger}_{-\mathbf{R}}(t)\hat{O}^{\alpha}_{\mathbf{0}}(0)\rangle\right)^*\right] dt \\ &= \frac{1}{2\pi}\sum_{\mathbf{R}} e^{-i\mathbf{k}\cdot\mathbf{R}} \int_0^{\infty} \left[e^{i\omega t}\langle\hat{O}^{\alpha\dagger}_{\mathbf{R}}(t)\hat{O}^{\alpha}_{\mathbf{0}}(0)\rangle + \left(e^{i\omega t}\langle\hat{O}^{\alpha\dagger}_{\mathbf{R}}(t)\hat{O}^{\alpha}_{\mathbf{0}}(0)\rangle\right)^*\right] dt \\ &= \frac{1}{2\pi}\sum_{\mathbf{R}} e^{-i\mathbf{k}\cdot\mathbf{R}} \int_0^{\infty} 2\mathrm{Re}\left[e^{i\omega t}\langle\hat{O}^{\alpha\dagger}_{\mathbf{R}}(t)\hat{O}^{\alpha}_{\mathbf{0}}(0)\rangle\right] dt \end{aligned}$$

Discretized time steps Notice that up to this point we are discussing the exact formula, this is the first place where we consider an approximation. To put the computation on a computer, instead of considering continuous time steps, we only evaluate discrete time steps. That is we *approximate* the integral by summation.

In addition to discrete time steps, we would only evolve the state to a finite time T. The cutoff time T is considered for different reasons. Firstly, we could not consider infinite time steps on a computer running for finite time. Secondly, in practice, we often simulate the finite systems with open boundary condition. That is we approximate the translational invariant systems with periodic boundary condition by systems with open boundary condition. If we did this, we do not want the excitation "spread" to the boundary such that boundary effect shows up.

Considering a finite time cutoff has the effect that we will lose details about low frequency information, which corresponds to the most important low energy excitations. You will see this effect in the exercises below. Moreover, the time signal we use for the Fourier transform is then the true time evolution of the system convoluted with a rectangular function of finite length (in time). Fourier transforming such a rectangular function leads to Gibbs oscillations which would also strongly show up in the numerical results of the spectral functions. This can be improved by applying a Gaussian window function (cf. next paragraph).

Remedy We see there are several approximation we made in order to carry out the calculation. (i) We approximate the ground state and the time-evolved states by tensor networks. (ii) We perform time evolution by discretizing the time evolution operators. (iii) We discretize the integral to summation. (iv) We cutoff the summation to finite time T. The first error could be controlled by increasing the bond dimension of the tensor networks. The second and third error could be made smaller by considering smaller time steps or higher order Trotterization.

To prevent the Gibbs oscillations mentioned above from appearing in the numerically calculated dynamic structure factor, we can, instead of Fourier transforming the truncated time series in a finite time window, transform the time series convoluted with a Gaussian window function:

$$G(t_n) = e^{-\frac{1}{2}\cdot\left(\frac{t_n}{\sigma N}\right)^2}. \tag{7}$$

Here, N denotes the total number of time steps and t_n iterates over all time steps in the time series (e.g. $t_n = 0, \ldots, N$ for $t \in [0, \Delta t \cdot N]$). σ is the width of the distribution and should be chosen as $\sigma \lesssim 0.5$.

Since this procedure leads to comparably lower weight for the numerically expensive time evolution steps at large times, one can improve this method by extending the computed time series from the MPS time evolution via linear prediction methods to notably larger times (e.g. factor 5) such that the weight of the Gaussian window fades out on the linearly predicted tail. This complication, however, can be skipped for these exercises.

1.4 Connection to Inelastic neutron scattering

The considerations so far have already been highly interesting from a theorist's point of view since the method presented allows to detect the excitations of a quantum system. However, the dynamic spin structure factor can also be probed directly in neutron scattering experiments [7, 17, 18]. The cross-section for scattering neutrons obeys the following relation [17, 18]

$$\frac{d^2\sigma(\mathbf{k},\omega)}{d\omega d\Omega} \propto \sum_{\alpha,\beta} \underbrace{\left(\delta_{\alpha,\beta} - \frac{k_\alpha k_\beta}{|\mathbf{k}|^2}\right)}_{\text{polarization factor}} \times \underbrace{F(\mathbf{k})^* F(\mathbf{k})}_{\substack{\text{magnetic} \\ \text{form factors}}} \times S^{\alpha\beta}(\mathbf{k},\omega) \tag{8}$$

The magnetic form factor depends on the details of the atomic or molecular orbitals of the sample. An additional Debye-Waller factor could be included to take into account the effect of phonons and lattice distortions. However, we see that the measurable cross-section is directly related to the dynamic structure factor. Figure 1

presents a direct comparison of experimental data with numerical calculations using the methods presented above [7].

2 Numerical Procedure

Using the methods discussed above, we can now obtain spectral functions for concrete physical systems. The system we are interested in is the quantum Ising chain with a transverse and a longitudinal field as considered already in the first part of this project:

$$H = -J \sum_n \sigma_n^x \sigma_{n+1}^x - g \sum_n \sigma_n^z - h \sum_n \sigma_n^x. \tag{9}$$

2.1 Dynamical spin structure factor

a) Use the TEBD algorithm to write some code that performs a time evolution and calculates correlation functions of the form

$$C(t, j) = \langle \psi_0 | \, e^{\mathrm{i}Ht} \sigma_j^y e^{-\mathrm{i}Ht} \sigma_{L/2}^y \, | \psi_0 \rangle \, ,$$

where $|\psi_0\rangle$ is the ground state of the transverse field Ising model. During the time evolution, make sure to save the bipartite von-Neumann entanglement entropy

$$S(t) = -\sum_\alpha \Lambda_\alpha^2(t) \ln \left(\Lambda_\alpha^2(t) \right) \, ,$$

where Λ_α are the Schmidt values on the bond at the center of the time evolved state $|\psi(t)\rangle = e^{-iHt} \sigma_{L/2}^y |\psi_0\rangle$.

b) Write another function that performs a Fourier transformation in space and time to obtain the dynamic structure factor $S(k, \omega)$:

$$S(k, \omega) = \sum_{j=0}^{L-1} \sum_{t_n=0}^{N} e^{i\omega \, \Delta t \cdot t_n - ik \cdot j} \, C(\Delta t \cdot t_n, j) \cdot G(t_n)$$

Remember to multiply the signal with a Gaussian window function $G(t_n)$ in order to avoid Gibbs oscillations from the Fourier transform of the finite time data (cf. equation (7)).

c) Perform a time evolution at $g = 0.2$ and $g = 2$ with $h = 0$. For this task, we choose the total time T such that the excitation does not spread to the boundary

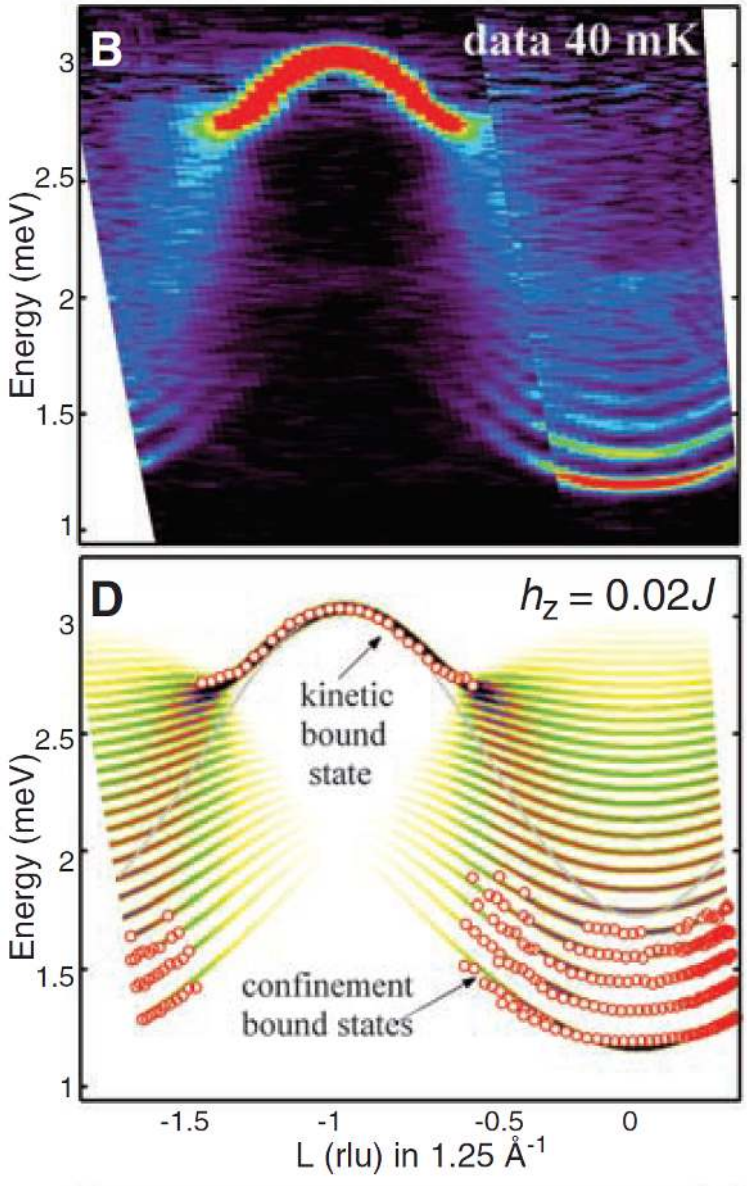

Figure 1: Measurement (B) and model calculation (D) of bound states in $CoNb_2O_6$ (from [7]).

yet. To check this, plot the correlations $C(t, j)$ as a colorplot in dependence of time and the spatial variable j. Make a similar plot for the bipartite von Neumann entanglement entropy $S(t)$. What do you observe?

Hint: You can choose for instance $L = 30$, $T = 25\,J$ and $L = 50$, $T = 10\,J$ for the cases $g = 0.2$ and $g = 2$ respectively.

Obtain $S(k, \omega)$ from $C(t, j)$ using your code from part (b). How do the spectral functions in the two cases compare?

Feel free to play around with the parameters of the simulation such as system size L, total simulation time T and time step size Δt to improve the quality of your plots.

d) Obtain $S(k, \omega)$ at $g = 0.2$ and $h = 0.1$. How does the picture change compared to (c)? At low transverse field and small bound state momentum, the system can be described by a one-dimensional Schrödinger equation with a linear confining potential with the energy levels given by the negative zeros of the Airy function. Compare the bound states you find in your numerics with the zeros of the Airy function.

References

[1] E. Schrödinger, Proceedings of the Cambridge Philosophical Society **31**, 555 (1935)

[2] A. Einstein, B. Podolsky, and N. Rosen, Phys. Rev. **47**, 777 (1935)

[3] S. R. White, Phys. Rev. Lett. **69**, 2863 (1992)

[4] G. Vidal, J. I. Latorre, E. Rico, and A. Kitaev, Phys. Rev. Lett. **90**, 227902 (2003)

[5] G. Vidal, Phys. Rev. Lett. **93**, 040502 (2004)

[6] G. Vidal, Phys. Rev. Lett. **98**, 070201 (2007)

[7] R. Coldea, D. A. Tennant, E. M. Wheeler, E. Wawrzynska, D. Prabhakaran, M. Telling, K. Habicht, P. Smeibidl, and K. Kiefer, Science **327**, 177 (2010)

[8] D. N. Page, Phys. Rev. Lett. **71**, 1291 (1993)

[9] M. B. Hastings, J. Stat. Mech. Theory Exp. **2007**, P08024 (2007)

[10] M. Fannes, B. Nachtergaele, and R. F. Werner, Commun. Math. Phys. **144**, 443 (1992)

[11] U. Schollwöck, Ann. Phys. (N. Y). **326**, 96 (2011)

[12] D. Gottesman and M. B. Hastings, New J. Phys. **12**, 025002 (2010)

[13] N. Schuch, M. M. Wolf, F. Verstraete, and J. I. Cirac, Phys. Rev. Lett. **100**, 030504 (2008)

[14] M. Suzuki, J. Math. Phys. **32**, 400 (1991)

[15] J. Eisert, M. Cramer, and M. B. Plenio, Rev. Mod. Phys. **82**, 277 (2010)

[16] B. M. McCoy and T. T. Wu, Phys. Rev. D **18**, 1259 (1978)

[17] I. A. Zaliznyak, and S. H. Lee: Magnetic neutron scattering. In: Zhu Y. (eds) Modern Techniques for Characterizing Magnetic Materials. Springer, Boston, MA. (2005)

[18] R. Verresen: Topology and Excitations in Low-Dimensional Quantum Matter (2019). Doctoral thesis.